



# Electrochemical and spectroelectrochemical analyses of hydrothermal carbon supported nickel electrocatalyst for ethanol electro-oxidation in alkaline medium



A. Cuña <sup>a,b,\*</sup>, C. Reyes Plascencia <sup>a</sup>, E.L. da Silva <sup>b</sup>, J. Marcuzzo <sup>c</sup>, S. Khan <sup>b</sup>, N. Tancredi <sup>a</sup>, M.R. Baldan <sup>c</sup>, C. de Fraga Malfatti <sup>b</sup>

<sup>a</sup> Cátedra de Fisicoquímica, DETEMA, Facultad de Química, Universidad de la República, Avenida General Flores 2124, CC 1157, Montevideo, 11800, Uruguay

<sup>b</sup> LAPEC/PPGE3M, Universidade Federal do Rio Grande do Sul, Av. Bento Gonçalves, 9500, setor 4, prédio 75, sala 232, 91501-970, Porto Alegre, RS, Brazil

<sup>c</sup> Laboratório Associado de Sensores e Materiais, Instituto Nacional de Pesquisas Espaciais, 12245-010, São José dos Campos, SP, Brazil

## ARTICLE INFO

### Article history:

Received 7 April 2016

Received in revised form 18 August 2016

Accepted 30 August 2016

Available online 31 August 2016

### Keywords:

Direct ethanol fuel cells

Hydrothermal liquefaction

Nickel catalyst

Ethanol electro-oxidation

Spectroelectrochemical analysis

## ABSTRACT

This paper presents the study of a simple and fast method to prepare an activated hydrothermal carbon supported nickel electrocatalyst (Ni/aHC) for ethanol oxidation reaction (EOR) in alkaline medium. The cyclic voltammogram obtained for the Ni/aHC sample in a 1.0 mol L<sup>-1</sup> NaOH solution shows an anodic and a cathodic peak. These redox couple reaction peaks can be related to the reversible formation of (NiO)OH. The catalytic activity of the Ni/aHC sample regarding the EOR is clearly evident from the cyclic voltammogram obtained in presence of ethanol, where a significant increase in the current density from 0.55 V vs. Hg/HgO is observed. This potential value, related with the onset potential ( $E_{onset}$ ) of the EOR, is very close to the corresponding (NiO)OH formation potential, confirming that this species is directly involved in the EOR on the Ni/aHC electrocatalyst. The *in-situ* Attenuated Total Reflectance FTIR (*in-situ* ATR-FTIRS) spectra of this sample show two intense peaks related with acetate ion formation. Based on the ATR-FTIRS and electrochemical analyses, and in the literature information, a reaction pathway of the EOR on Ni/aHC in alkaline medium is proposed.

© 2016 Elsevier B.V. All rights reserved.

## 1. Introduction

In recent years, the research of alkaline fuel cells (FCs) has received a significant attention [1–6]. The most important advantages of alkaline FCs are their faster fuel oxidation and oxygen reduction reactions as compared to the acidic FCs. The inherently faster kinetics in alkaline FCs allow the use of non-noble and low-cost metal electrocatalysts such as silver and nickel, making them potentially low cost in comparison to others fuel cells types that use platinum based electrocatalysts [6]. In addition, the use of a non-Pt electrocatalyst on the cathode eliminates the oxidation of the fuel that may be transported from the anode, which makes the cathodic potential much higher than that in acidic FCs [7]. Besides, the exchange membranes used in alkaline FCs have lower fuel permeability and allow better water management. Thus that simplifies

the cell design, since the ionic current happens due to the hydroxide ions conduction [4–6].

On the other hand, the use of liquid fuels in direct alcohol fuel cells (DAFCs), such as low-molecular weight alcohols (methanol, ethanol and others) [8,9], has several further advantages compared to the use of pure hydrogen, because liquid fuels can be easily handled, stored and transported. In particular, the use of ethanol has several advantages, such as its high energy density, higher solubility in liquid electrolytes, low cost and availability. Furthermore, ethanol is a non-toxic fuel, and it can be produced in large quantities by the fermentation process of sugar-containing biomass or agricultural products. Therefore, direct ethanol fuel cells (DEFCs) have attracted considerable interest for their technological application as alternative power sources for automobile and portable consumer electronics, among others [10].

All aforementioned advantageous features highlight a strong potential for the research and development of alkaline DEFCs that present a great interest for the scientific community. In the last years, several works related to the design and performance of the alkaline DEFCs have been conducted by Li et al. [7,11,12,13–15]. In these works, particular attention was paid to investigating the

\* Corresponding author at: Cátedra de Fisicoquímica, DETEMA, Facultad de Química, Universidad de la República, Avenida General Flores 2124, CC 1157, Montevideo, 11800, Uruguay.

E-mail address: [acuna@fq.edu.uy](mailto:acuna@fq.edu.uy) (A. Cuña).

effects of different operating parameters, including the cell operating temperature, concentrations of both ethanol and the base electrolyte solution, the design of the electrodes materials and electrodes architecture, and to the study of anion-exchange membrane durability.

One of the current challenges in the alkaline DEFCs research area is to develop an electrocatalyst that maximizes the efficiency and the ethanol oxidation reaction (EOR) rate in the cell anode, and, if possible EOR should be performed using non-noble less expensive metals as electrocatalysts [3,6]. In this context, supported bimetallic Pd-M (M=Ru, Au, Sn and Cu) catalysts [16–19], the addition of various oxides to carbon supported Pt and Pd catalysts [19–21] and Ru-Ni and Ru-Ni-Co catalysts [22–24] have been tested for EOR in alkaline media. Considering its low cost and chemical safety, in recent years, pure nickel [2] or nickel based nanocomposites [25,26] have been tested for EOR in alkaline medium. These studies have shown that nickel is an important candidate to be used as catalyst for the EOR although there is still plenty of room to improve its electrocatalytic performance and to explore simpler and a low cost synthesis routes. Moreover, some aspects of the EOR mechanism using nickel based electrocatalyst in alkaline medium warrant further exploration for its better physico-chemical understanding.

In addition to the catalyst, another important component in the electrocatalyst preparation is the catalyst support. The essentials to the catalyst supports for electro-oxidation are their high electrical conductivity, high surface area and chemical stability [27,28]. Among the different classes of electrocatalyst test in the literature, studies have attracted special attention and indicated that carbon materials are one of the most important groups of materials used as catalyst supports and different type of these materials have been investigated and employed for this application [27–35]. In recent years, the preparation of carbon materials from wood has been studied for their application as support in electrocatalysts for EOR [31] and other applications such as an active material in supercapacitors electrodes [36,37]. Hydrothermal liquefaction (HTL) is an aqueous process, in an inert atmosphere, moderate temperature (250–550 °C) and high pressure (5–20 MPa), used for producing a liquid biofuel known as bio crude. In this process a gas phase and a solid phase rich in carbon, called hydrothermal carbon (HC), are also produced [38–41]. HCs may also have interesting properties as a catalyst support [42,43].

Another issue that still needs to be addressed is the reaction mechanism and the identification of formed products associated with the EOR on different electrocatalysts in alkaline electrolytes. *In-situ* Fourier Transform Infrared Spectroscopy (*in-situ* FTIRS) is a dynamic technique that can allow the study of the physicochemical changes in a solid/liquid interface as a function of an external electric field [44,45]. *In-situ* FTIRS has been successfully used to obtain qualitative and quantitative data on electrochemical surface processes, such as electro-oxidation of small organic molecules [45]. The *in-situ* FTIRS can be carried out using different variations, one of them is the technique *in-situ* FTIRS in the Attenuated Total Reflectance mode (*in-situ* ATR-FTIRS), which is an appropriate technique to perform *in-situ* FTIRS measurements for non-reflective surfaces like the carbon supported catalysts [46]. In recent years, some authors have reported the use of *in-situ* ATR-FTIRS, following different methodologies, to study the EOR mechanism pathways in acidic [47–51] or alkaline medium [4,26] and to determine the product distributions at different potentials. So far, EOR mechanism studies for hydrothermal carbon supported nickel based electrocatalysts using alkaline base electrolyte have not been reported.

In this work, a new, simple, fast, low cost and environmental friendly route was applied for hydrothermal carbon supported nickel electrocatalyst preparation. The morphology, structure and chemical composition of the prepared electrocatalyst were determined by X-ray diffraction (XRD), transmission electron

microscopy (TEM) and X-ray photoelectron spectroscopy (XPS). These properties were correlated to their electrocatalytic performance in EOR, and by *in-situ* ATR-FTIRS, with the EOR mechanism pathways and product distributions at different potentials, using 1.0 mol L<sup>-1</sup> ethanol + 1.0 mol L<sup>-1</sup> NaOH as solution.

## 2. Experimental

### 2.1. Samples preparation

Activated hydrothermal carbon supported Ni electrocatalyst was prepared according to the scheme of Fig. 1. The *Eucalyptus globulus* wood hydrothermal liquefaction (HTL) was carried out in a stainless steel Parr (model 4575) batch reactor with continuous agitation of 150 rpm. The reactor was purged with N<sub>2</sub> prior to reaction in order to remove the oxygen. HTL was performed using a 0.54 mol L<sup>-1</sup> Ni(NO<sub>3</sub>)<sub>2</sub> aqueous solution. The solution/wood relation was 1/6 (w/w). The HTL was carried out at 350 °C in a vapor pressure of 2500 ± 37 psi during 30 min. After the reaction the reactor was cooled and the reaction gases were released. The liquid and solid phases were separate by filtration, and the solid phase was washed with distilled water and finally dried at 100 °C until the final product reaches a constant weight. This solid phase corresponds to the hydrothermal carbon supported NiO (NiO/HC). The obtained NiO/HC was then submitted to thermal and CO<sub>2</sub> activation treatments. The treatments were carried out in a horizontal Carbolite (CTF 12/75) furnace according to the following steps: a) Heating rate of 5 °C min<sup>-1</sup> in a N<sub>2</sub> atmosphere at a constant flow of 200 mL min<sup>-1</sup>, b) once reached 800 °C, the gas flow was shifted to 200 mL min<sup>-1</sup> of CO<sub>2</sub> and it was left for 1 h and c) After activation time, the oven was cooled until ambient temperature in a flow of N<sub>2</sub>. After all the process steps have been completed an activated hydrothermal carbon supported Ni electrocatalyst (Ni/aHC) was obtained.

Another hydrothermal carbon samples were obtained only to be used in the termogravimetric analysis (TGA) for comparative purposes. These samples were prepared in the same way and under the same conditions as above mentioned. The only difference was that for the hydrothermal carbon samples, the HTL was performed in absence of Ni(NO<sub>3</sub>)<sub>2</sub>. Thus, the hydrothermal carbon (HC) and the activated hydrothermal carbon (aHC) were obtained.

### 2.2. Structural, morphological and chemical characterization

X-Ray diffraction (XRD) analyses were made with a Rigaku model Ultima IV equipment. The wave longitude was 1.54 Å corresponding to K $\alpha_1$  radiation of Cu. X-Ray diffractogram allows establishing the phase and the crystal structure assumed by the Ni and NiO on the hydrothermal carbon support. Morphological information for the samples was obtained with a JEOLJEM 2010 TEM, operating at 200 kV. The interplanar spacing was determined by Digital Micrograph.

X-ray photoelectron spectroscopy (XPS) has proved to be a powerful method for the investigation of surface chemistry. XPS surface characterization method combines surface sensitivity with the ability to quantitatively obtain both elemental and chemical state information. All the XPS measurements were carried out with a Kratos Axis Ultra XPS spectrometer using a monochromated Al-K $\alpha$  (1486.5 eV) X-ray radiation at a power of 15 kV at 150 W. The emitted photoelectrons were detected using a hemispherical analyser and 15  $\mu$ m spatial resolution. The vacuum system was maintained at approximately 10<sup>-9</sup> Torr during all the experiments. Survey scans were collected from 0 to 1100 eV with a pass energy equal to 160 eV with step size of 1 eV, in order to identify the ele-

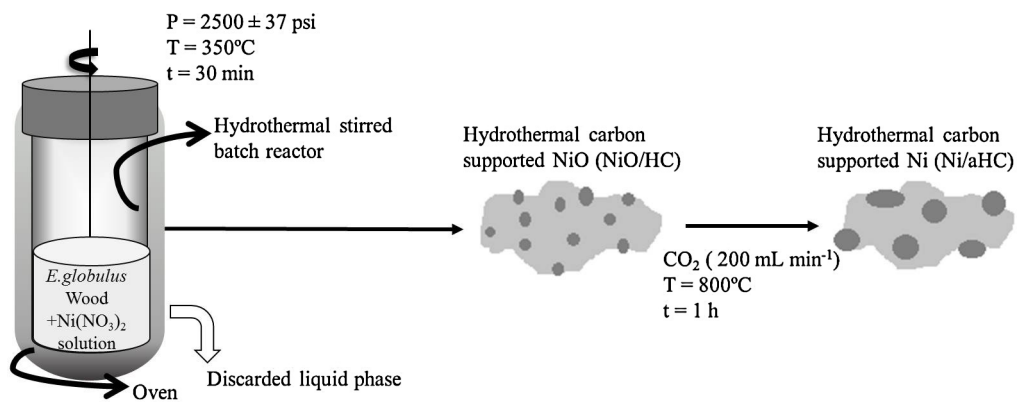


Fig. 1. Scheme of the experimental procedure for the Ni/aHC electrocatalyst preparation.

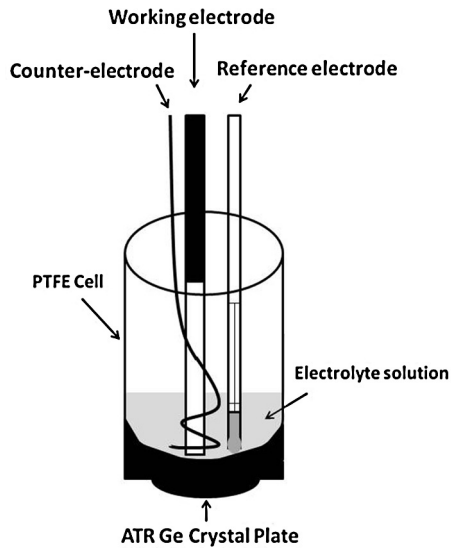


Fig. 2. Experimental arrangement for cyclic voltammetries and for *in-situ* ATR-FTIR measurements.

ments present on the surface, and a pass energy of 40 eV for high resolution scans on specific atomic peaks.

Thermogravimetric analysis (TGA) was performed on the samples using a Shimadzu TG-50 equipment in a dynamic air atmosphere, in the temperature range of 25–900 °C, at constant heating rate of 5 °C min<sup>-1</sup>, with sample masses between 8.0 and 10.0 mg in platinum crucible.

### 2.3. Electrochemical characterization

The electrochemical measurements were carried out in order to determine the electrochemical behavior of the electrocatalysts in a 1.0 mol L<sup>-1</sup> NaOH solution and in 1.0 mol L<sup>-1</sup> ethanol + 1.0 mol L<sup>-1</sup> NaOH solution. Measurements were carried out at room temperature in a standard three-electrode cell connected to a potentiostat/galvanostat AUTOLAB PGSTAT 302N, as described in Fig. 2. All the potentials were measured with respect to Hg/HgO as a reference electrode, and a platinum wire as counter-electrode. As working electrode a graphite disk was used. Its geometric area was 0.29 cm<sup>2</sup>, and it was coated with a suspension of 1.65 mg of electrocatalyst powder in Nafion®. The experiments were performed with a scan rate of 50 mV s<sup>-1</sup> in a potential range from 0.1 to 0.8 V vs. Hg/HgO electrode. Chronoamperometry experiments were performed using 1.0 mol L<sup>-1</sup> ethanol + 1.0 mol L<sup>-1</sup> NaOH solution at 0.6, 0.7 and 0.8 V over 30 min. All the solutions were deaerated by N<sub>2</sub>

purging during 10 min prior to the measurements. In order to avoid the oxygen presence in the medium, nitrogen stream was led inside the solution during all the electrochemical experiments.

### 2.4. Spectroelectrochemical experiments

The spectroelectrochemical *in-situ* ATR-FTIR measurements in 1.0 mol L<sup>-1</sup> NaOH + 1.0 mol L<sup>-1</sup> ethanol solution were carried out at 25 °C using a Bruker Vertex 70V spectrometer equipped with a Mercury-Cadmium-Telluride (MCT) detector cooled with liquid N<sub>2</sub> and ATR Ge crystal plate. ATR Ge window was used because it was suitable for these experiments from the point of view of chemical resistance to the electrolyte solution used and it allows adequate detection of the most important FTIR bands for all EOR expected products. The experimental setup used in this work was similar to that used by De Souza et al. [46], using the same three-electrode cell that were used in electrochemical experiments. The spectra were collected as the ratio R:R<sub>0</sub>, where R represents a spectrum at a given potential, and R<sub>0</sub> is the spectrum collected at 0.0 V vs. Hg/HgO electrode. Positive and negative directional bands represent gains and losses of species at the sampling potential, respectively. The spectra were computed from 96 interferograms averaged from 4000 cm<sup>-1</sup> to 800 cm<sup>-1</sup> with the spectral resolution set to 4 cm<sup>-1</sup>. Initially, a reference spectrum (R<sub>0</sub>) was measured at 0.0 V, and then sample spectra were collected after applying successive potential steps from 0.1 to 0.8 V vs. Hg/HgO electrode.

## 3. Results and discussion

### 3.1. XRD and TGA analyses

The X-ray diffraction (XRD) diffractograms of the prepared samples are compared in Fig. 3. For NiO/HC the peaks at 37.0°, 43.0° and 62.8° are indexed as (111), (200) and (220) crystal planes of NiO [52]. The low intensities and the width of the peaks suggest a small NiO crystal size [52]. The NiO formation in the first stage of the preparation route studied in this work can be associated with the thermal decomposition of the nickel salt during the HTL [53–56]. From these results, it can be confirmed that the first stage of our proposed method is feasible for an easy preparation of NiO particles supported on hydrothermal carbon material. Therefore, besides being the precursor to obtaining a nickel hydrothermal supported electrocatalyst, the NiO/HC sample can be used in other energy applications such as active material in supercapacitor electrodes [55,57,58] and anode of lithium-ion batteries [52].

For Ni/aHC sample, that shows peaks at 44.4° and 51.8° correspond to the (111) and (200) facets of Ni<sup>0</sup> crystal [65,59–61]. Other small peaks can be seen at 37.0°, 43.0° and 62.8° indicating small

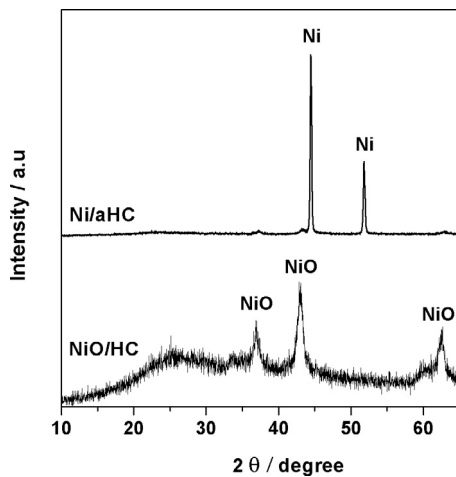
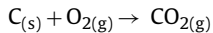
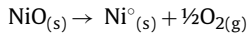


Fig. 3. X-ray diffraction patterns of Ni/aHC and NiO/HC samples.

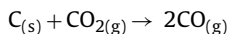
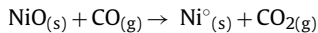
amounts of remanent NiO particles. The intensity of the Ni° peaks are clearly higher intense than those corresponding to NiO which prove the quasi-total conversion of NiO particles in Ni° after the treatment performed on the NiO/HC sample.

This conversion can be explained as follows: as indicated in the experimental procedure, the sample NiO/HC was submitted to a thermal treatment and subsequent activation with CO<sub>2</sub> at 800 °C. When NiO particles and a material with high percentage of carbon are submitted together to a thermal treatment at higher temperatures (above 700 °C) under inert atmosphere or in the presence of CO<sub>2</sub> atmosphere, the NiO particles reacts with carbon through any of the following carbothermal reduction mechanisms [56,62]:

Thermal dissociation mechanism



Oxide reduction through intermediates gases



In the latter mechanism, the presence of CO<sub>(g)</sub> is necessary for the NiO conversion, therefore, a rather restoration of CO from the second reaction of the mechanism can be an important limitation for this [62]. However, in our experimental procedure, the restoration of CO would be favored by the CO<sub>2</sub> atmosphere imposed in the second stage of the procedure.

On the other hand, at temperatures above 700 °C, CO<sub>2</sub> can act as an activating agent of carbon materials generating micro and mesoporosity [63]. In addition, it is well known that the heat treatment at temperatures above 700 °C can improve the electrical conductivity of the biomass derived carbon materials [37]. These effects are very good from the point of view of the use of material as a catalyst support, because, high specific surface area and good electrical conductivity are two of the most important characteristics that a material should have to be used as a catalyst support in the electrocatalysts preparation [27,28].

TGA curve in air atmosphere obtained from the NiO/HC and HC samples are shown in Fig. 4. Taken into account that, during the TGA the NiO present in the NiO/HC sample does not react with oxygen [56] and the HC support completely react (see HCTGA curve in Fig. 4). The NiO mass content of 32.3% was determined from the remaining mass in the TGA curve of the NiO/HC sample. On the other hand, the TGA curve of the Ni/aHC (Fig. 4) shows a mass

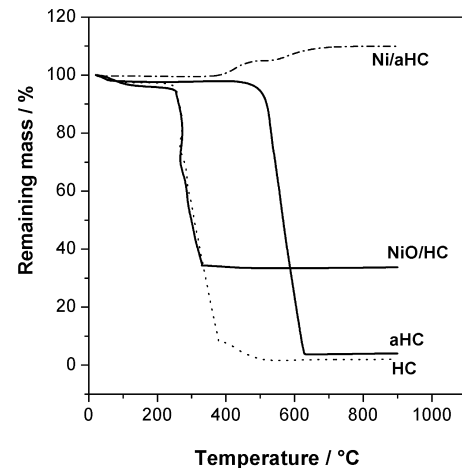


Fig. 4. TGA curves in air atmosphere of the prepared samples.

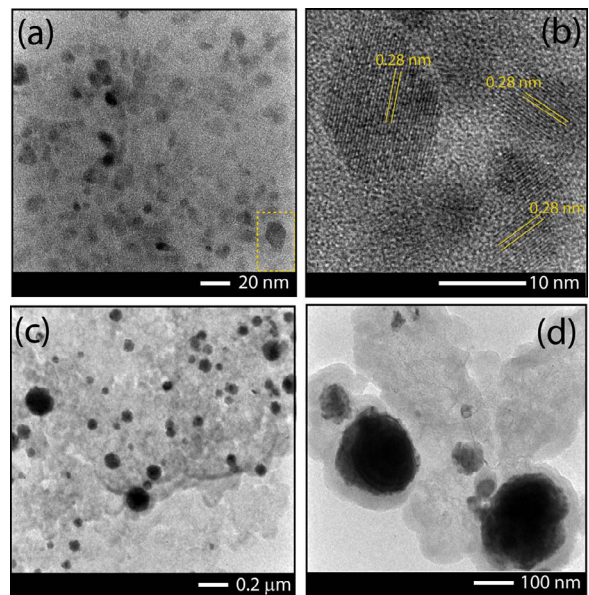


Fig. 5. Micrograph obtained from TEM of NiO/HC (Figures a and b) and Ni/aHC (Figures c and d).

increase at 355 °C, while in the TGA curve of the aHC support a clear decrease was observed (Fig. 4). These facts suggest the formation of nickel oxide from Ni° particles [56] present on the hydrothermal carbon surface during the TGA of the Ni/aHC sample. This result also confirms the presence of Ni° in the Ni/aHC sample which is consistent with the XRD results.

### 3.2. TEM and XPS analyses

The TEM micrographs presented in Fig. 5a shows NiO nanoparticles of ca. 8.2 nm. A zoom of a selected area (marked with a yellow rectangle) in Fig. 5a is shown in Fig. 5b. From this figure it is possible to determine the interplanar spacing of 0.28 nm (see the yellow marked lines in figure) which is consistent with the d<sub>200</sub> of face centered cubic NiO [64].

TEM micrographs of Ni/aHC sample are shown in Fig. 5c and d. These figures evidence the formation of larger particles reaching an average size of 58.9 nm. Taking into account the results of XRD and TGA analyses, the particles observed in the Ni/aHC may be associated to Ni° particles. These large Ni° particles could be the

**Table 1**

Surface chemical composition obtained from the XPS analyses.

Sample	Emission line	Binding energy/eV	Attributed species
NiO/HC	Ni 2p <sub>3/2</sub>	853.3	NiO
		529	NiO
		532.8	—C=O
	C 1s	284.1	C—C
		286.9	C=C
		291.7	—C=O
		852.7	Ni
Ni/aHC	Ni 2p <sub>3/2</sub>	853.9	NiO
		855.9	Ni <sub>2</sub> O <sub>3</sub>
		529.5	NiO
	O 1s	531.3	Ni <sub>2</sub> O <sub>3</sub>
		532.6	—C=O
		284.6	C=C
		285.7	C—C
		289	—C=O

result of the previous coalescence of smaller NiO particles during the thermal and activation treatments of the NiO/HC sample.

The information about the surface chemical composition of the samples was obtained from the XPS peak fitting. A comparison of the results were summarized in **Table 1**. The XPS detail spectrum of the Ni 2p<sub>3/2</sub> emission line was fitted with two peaks (**Fig. 6a**). The peak at 853.3 eV and its satellite at 859.2 eV were assigned to a NiO species [2,58,65,66–68]. From the fit of O 1s emission line (**Fig. 6b**), the peaks at 529.0 eV and 532.8 eV were assigned to NiO species [58,66] and C—O/C=O bonds respectively [65]. Three peaks of the C 1s XPS spectrum are located at 284.1, 286.9, and 291.7 eV (**Fig. 6c**), corresponding to the C—C, C=C and —C=O bonds respectively [55]. The XPS analysis confirms the presence of NiO particles supported on hydrothermal carbon.

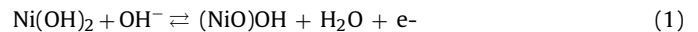
From the XPS spectra of the Ni/aHC sample (**Figs. 6d–f**), information about its surface chemical composition was obtained and has been summarized in **Table 1**. The peaks at 853.9 and 855.9 eV in the spectrum of Ni 2p<sub>3/2</sub> emission line and the peaks at 529.5 and 531.3 eV in the spectrum of O 1s emission line, indicate the presence of NiO [2,65–67] and Ni<sub>2</sub>O<sub>3</sub> [65,67] particles in the sample Ni/aHC. In the spectrum of the Ni 2p<sub>3/2</sub> emission, a small peak at 852.7 eV can be identified that corresponds to the presence of Ni<sup>0</sup> [2,65–67]. Interestingly, the XRD diffractogram of **Fig. 3** indicated the presence of Ni<sup>0</sup> in Ni/aHC. However, XPS analyses demonstrate the major contribution from nickel oxide species. It is reasonable to suggest that the surface of Ni<sup>0</sup> particles is coated with NiO and/or Ni<sub>2</sub>O<sub>3</sub> species and that are thick enough to appear in the XPS detection limit. On the other hand the Ni<sup>0</sup> phase exists underneath these species.

The structural and surface analyses show that through our proposed preparation method that it is possible to obtain a hydrothermal carbon supported Ni<sup>0</sup> nanoparticles (although with the coexistence of a small amount of NiO and/or Ni<sub>2</sub>O<sub>3</sub> particles). Future works should aim to achieve a complete conversion of the NiO into a Ni<sup>0</sup> particle, which could be achieved by fine tuning our synthesis procedures such as by increasing the time of the thermal and CO<sub>2</sub> treatments performed to the NiO/HC sample. It can be expected this should give more time to the NiO conversion according to the reactions involved in the carbothermal reduction mechanisms.

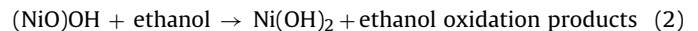
### 3.3. Electrochemical characterization in alkaline medium

The prepared Ni/aHC sample was evaluated as electrocatalyst for EOR in alkaline medium. **Fig. 7a** presents cyclic voltammetry of the Ni/aHC sample in 1.0 mol L<sup>−1</sup> NaOH solution. The sharp increase in oxidation current from 0.7 V vs. Hg/HgO towards the positive potentials can be related to oxygen evolution [69]. In the

voltammogram (**Fig. 7a**) is also clearly observed an anodic peak at 0.56 V and a cathodic peak at 0.35 V vs. Hg/HgO. These redox couple reactions have been linked to the formation and reduction of the surface oxide, which can be interpreted as the transition between the three-valent nickel oxyhydroxide and two-valent nickel hydroxide [2,6,70]:



As reported by Fleischmann et al. [70] and confirmed by Muench et al. [2], the nickel oxyhydroxide is the active chemical species in the oxidation of organic compounds such as methanol or ethanol on nickel catalyst. Therefore, nickel oxyhydroxide can participate in the EOR on the Ni/aHC electrocatalyst by the following reaction [2]:



The catalytic activity of the Ni/aHC sample regarding the EOR has been clearly evident in the voltammogram (**Fig. 7b**) that is obtained for Ni/aHC in 1.0 mol L<sup>−1</sup> NaOH + 1.0 mol L<sup>−1</sup> ethanol solution. A significant increase in the current density from 0.45 V vs. Hg/HgO towards more positive potentials can be observed that is clearly higher than the one determined in the cyclic voltammetry performed without ethanol (**Fig. 7a**). The value of 0.45 V, related with the onset potential (E<sub>onset</sub>) of the EOR, is very close to the corresponding (NiO)OH formation potential (0.47 V vs. Hg/HgO). It has been previously mentioned that the formation of this species is necessary for further EOR (Eq. (2)), therefore the lower potential of (NiO)OH formation is the lower E<sub>onset</sub> of EOR. The E<sub>onset</sub> value determined for the Ni/aHC sample is lower than the values determined by other authors for the EOR on different nickel electrocatalysts in alkaline medium [2,71]. These results suggest that Ni/aHC electrocatalyst has good qualities as a nickel based electrocatalyst for EOR in alkaline medium.

In order to quantify the additional currents corresponding to the EOR, the current densities of the Ni/aHC in 1.0 mol L<sup>−1</sup> NaOH solution during the cyclic voltammetry were subtracted from those recorded in the presence of ethanol (1.0 mol L<sup>−1</sup> NaOH + 1.0 mol L<sup>−1</sup> ethanol solution). The resultant voltammogram is shown in **Fig. 7c**. It can be seen that from 0.55 V vs. Hg/HgO the resultant net current density increases significantly until the maximum value of 28.5 mA cm<sup>−2</sup> at 0.71 V. This potential value (0.55 V) matches the value corresponding to the cathodic peak observed in **Fig. 7a**. This fact clearly confirms the direct relationship between the (NiO)OH formation and the EOR on the electrocatalyst.

Since with the used technique it is not possible to determine the mass percentage of Ni<sup>0</sup> present in the sample Ni/aHC, therefore, it is not possible to express the value of this maximum current density as a function of Ni<sup>0</sup> mass. However, for an approximation purpose, if we assume that the whole sample Ni/aHC consists of 100% Ni<sup>0</sup>, and considering the mass of the electrocatalyst sample used for the experiment (0.165 mg), the specific current density result is 50.1 A g<sup>−1</sup>. This value is higher than that reported for the EOR in alkaline medium using other electrocatalyst such as Pd/C [4], but is lower than reported for Pd–Ni electrocatalysts prepared by different methods and using different support materials. Various Pd–Ni electrocatalysts exhibited enhanced activity and greater tolerance to catalyst poisoning compared to pure Pd and current density up to 2831 A per gram of Pd has been achieved [72–75]. However, the key advantage of the Ni/aHC electrocatalyst over Pd–Ni electrocatalyst is that the prepared material in the current study is cost effective and does not require the use of an expensive noble Pd metal.

**Fig. 7d** shows the chronoamperometric curves for EOR on Ni/aHC electrocatalysts obtained by polarization at 0.6, 0.7 and 0.8 V vs. Hg/HgO for 30 min. These results are in agreement with the results obtained from the cyclic voltammogram (**Fig. 7b**), were in the potential range of 0.6–0.8 V, the current density is directly

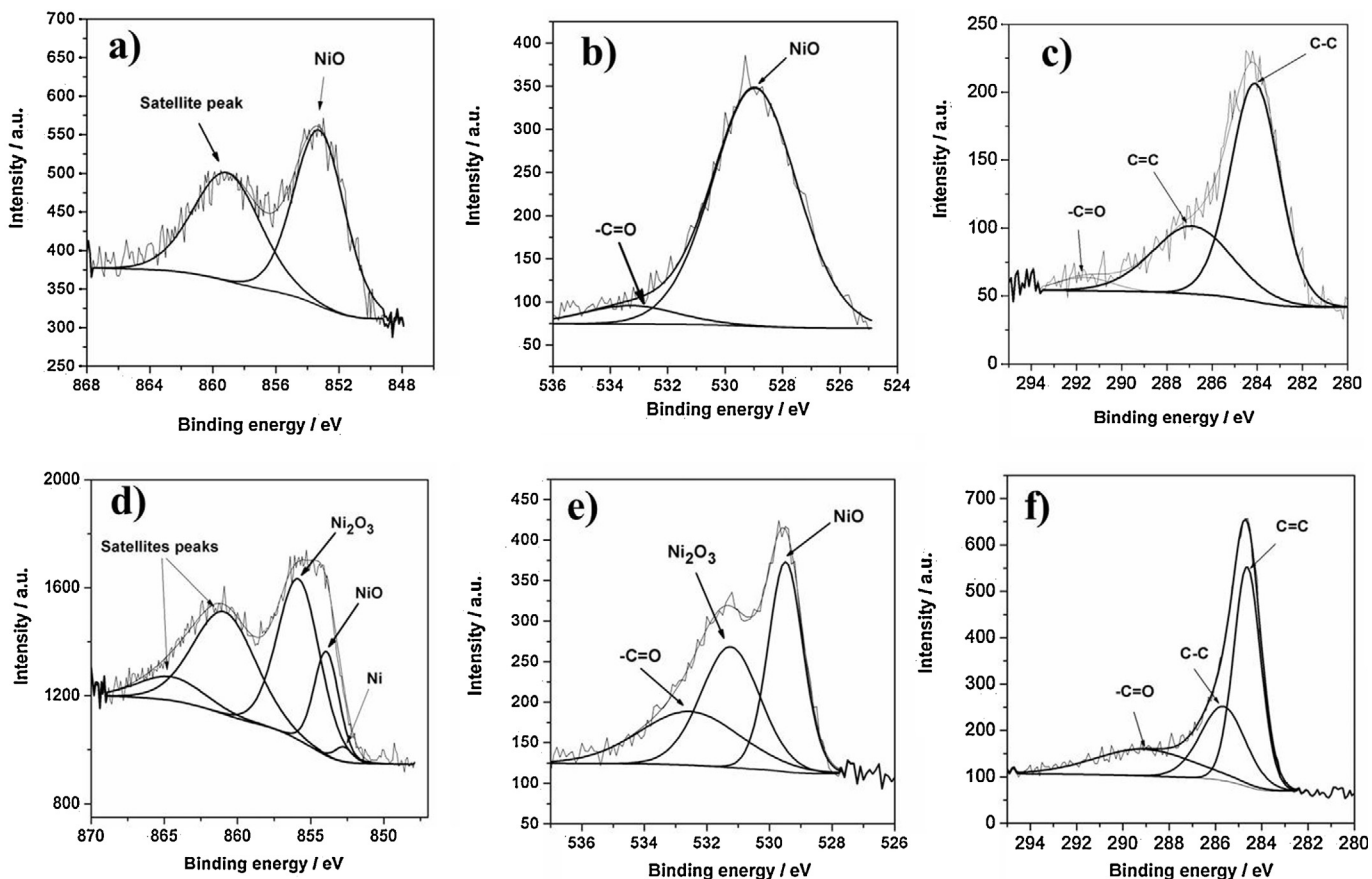


Fig. 6. Deconvoluted XPS spectra and the corresponding Ni 2p<sub>3/2</sub>, O 1s and C 1s regions of the NiO/HC and Ni/aHC samples.

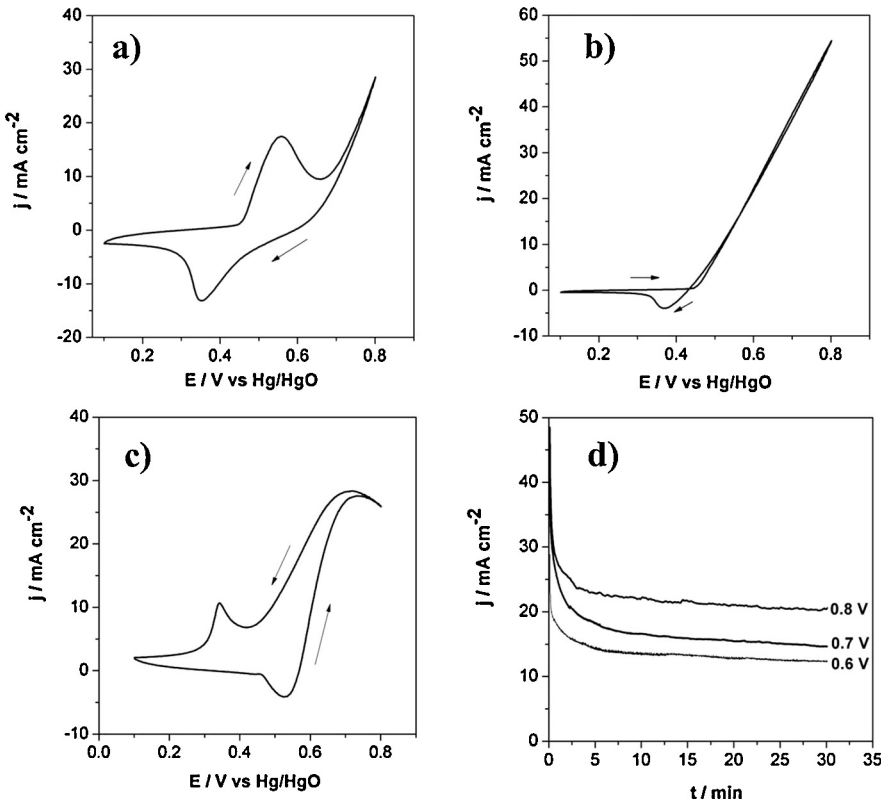
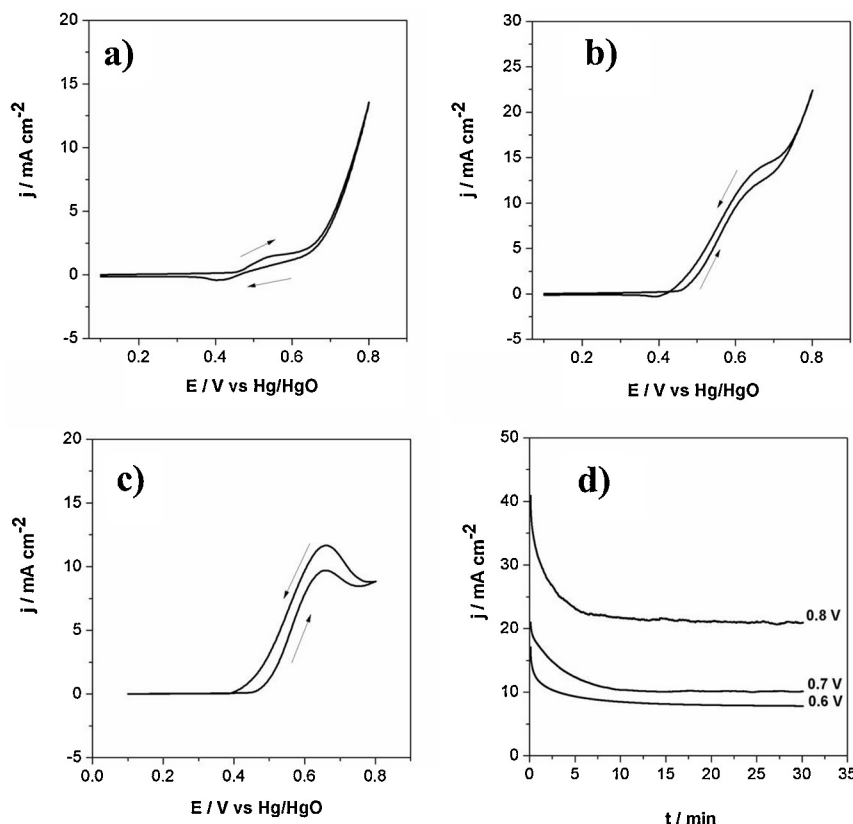


Fig. 7. (a) Cyclic voltammograms of the Ni/aHC sample at a scan rate of 50 mV s<sup>-1</sup> and T = 25 °C in 1.0 mol L<sup>-1</sup> NaOH and (b) 1.0 mol L<sup>-1</sup> NaOH + 1.0 mol L<sup>-1</sup> ethanol solutions. (c) Resultant voltammogram obtained by subtraction of the curve shown in (a) to the curve shown in (b). (d) Chronoamperometry curves for the Ni/aHC sample at different potentials in a 1.0 mol L<sup>-1</sup> NaOH + 1.0 mol L<sup>-1</sup> ethanol solution.



**Fig. 8.** (a) Cyclic voltammograms of the NiO/HC sample at a scan rate of 50 mV s<sup>-1</sup> and T = 25 °C in 1.0 mol L<sup>-1</sup> NaOH and (b) 1.0 mol L<sup>-1</sup> NaOH + 1.0 mol L<sup>-1</sup> ethanol solutions. (c) Resultant voltammogram obtained by subtraction of the curve shown in (a) to the curve shown in (b). (d) Chronoamperometry curves for the NiO/HC sample at different potentials in a 1.0 mol L<sup>-1</sup> NaOH + 1.0 mol L<sup>-1</sup> ethanol solution.

proportional to the applied potential. In Fig. 7d a gradual decrease in the oxidation current density with time is observed, which is generally attributed to the poisoning of the electrode by intermediates generated during EOR [5].

Fig. 8a shows the cyclic voltammetry in 1.0 mol L<sup>-1</sup> NaOH solution of the sample NiO/HC sample. This voltammogram presents a similar shape as was observed in the Ni/aHC sample, showing a sharp increase in the oxidation current from 0.7 V vs Hg/HgO related to oxygen evolution [76], an anodic peak at 0.47 V and a cathodic peak at 0.31 V vs. Hg/HgO. The main difference between NiO/HC and Ni/aHC samples, is that for the current density developed in the anodic and cathodic peaks is much lower than that current density determined for the Ni/aHC sample. This suggests that in the case of NiO/HC sample, the amount of the formed (NiO)OH (according to the reaction 2) is smaller than for Ni/aHC sample. Therefore a lower electrocatalytic activity of NiO/HC for EOR in alkaline medium is expected. This was confirmed by the cyclic voltammogram obtained for the NiO/HC sample in 1.0 mol L<sup>-1</sup> NaOH + 1.0 mol L<sup>-1</sup> ethanol solution (see Fig. 8b). It can be seen in Fig. 8b, the current density above 0.45 V vs. Hg/HgO does not increase much as it does for the sample Ni/aHC (see Fig. 7b). Fig. 8c shows the result of the voltammetry in presence of ethanol (1.0 mol L<sup>-1</sup> NaOH + 1.0 mol L<sup>-1</sup> ethanol solution) with the subtraction of that obtained in 1.0 mol L<sup>-1</sup> NaOH solution. It can be seen that from 0.50 V vs. Hg/HgO the resultant net current density increases significantly until the maximum value of 9.7 mA cm<sup>-2</sup> at 0.67 V. This value is lower than that obtained for the Ni/aHC, i.e. 28.5 mA cm<sup>-2</sup> at 0.71 V.

The chronoamperometric curves for obtained at different potentials polarization for the NiO/HC sample is shown in Fig. 8d. This

results show that the reactions at NiO/HC sample has similar stability behavior compared with the EOR at the Ni/aHC sample.

### 3.4. Spectroelectrochemical analysis

Aiming to identify the reaction products of the EOR on the Ni/aHC electrocatalyst (see Eq. (2)), *in-situ* ATR-FTIRS analysis was performed in alkaline medium at different potentials. Fig. 9a shows the spectra obtained at different potentials. From 0.5–0.6 V, two intense peaks are clearly observed, one located at 1413 cm<sup>-1</sup> and the other at 1553 cm<sup>-1</sup>. Both peaks are related to the presence of acetate ion (CH<sub>3</sub>COO<sup>-</sup>), and correspond to the symmetric and asymmetric C–O bond frequency vibrations [1,4,77]. In addition, a small peak at 931 cm<sup>-1</sup> can also be seen that is associated with O–C–O stretching of the hydrated form of acetaldehyde [78,79], and a negative peak at 1046 cm<sup>-1</sup> is associated with the ethanol [80] consumption. No peak was observed around 2342 cm<sup>-1</sup> associated with the presence of CO<sub>2</sub> [81]. However, the formation of CO<sub>2</sub> as a EOR product cannot be ruled out completely because as it is shown in the spectrum obtained at 0.8 V (Fig. 9a). The peak at 1413 cm<sup>-1</sup> has stretch and hump toward lower frequency values. This fact would indicate the presence of CO<sub>3</sub><sup>2-</sup>, which has a peak located at about 1370 cm<sup>-1</sup>, and it would come from the reaction of produced CO<sub>2</sub> with the OH<sup>-</sup> [1]. These results demonstrate that the acetate ion is the main product of EOR on the Ni/aHC electrocatalyst in the alkaline medium, which is also seen in other electrocatalysts types (Pd, PdAu, Pt) by *in-situ* FTIR experiments in alkaline medium [1,77].

The band intensities of acetate ion at 1413 and 1553 cm<sup>-1</sup>, and acetaldehyde at 931 cm<sup>-1</sup> as a function of the electrode potential are represented in Fig. 9b. Both band intensities for acetate ion rapid

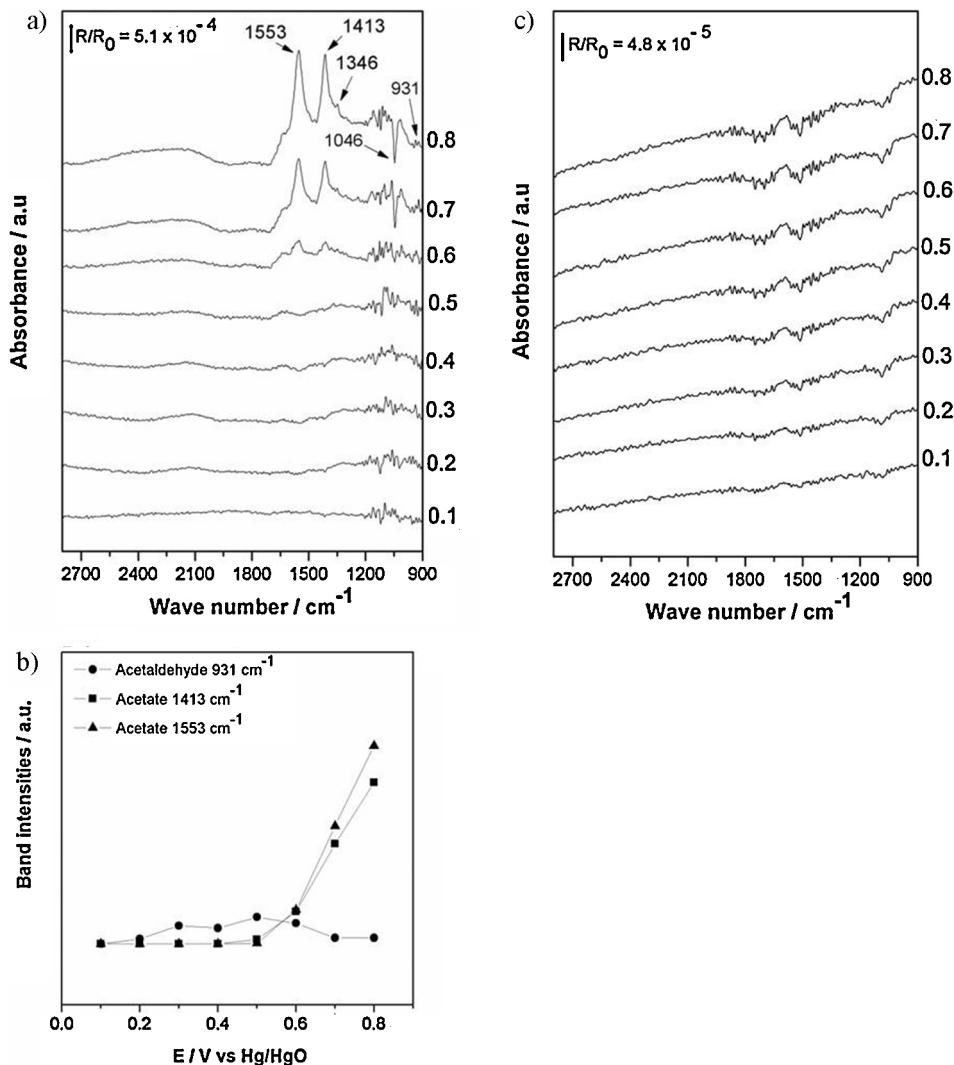
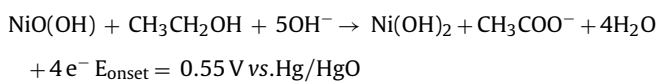
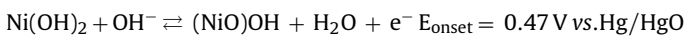


**Fig. 9.** *In-situ* ATR-FTIR spectra taken at several potentials (indicated in volts vs. Hg/HgO reference electrode on the right y-axis) in  $1.0 \text{ mol L}^{-1} \text{ NaOH} + 1.0 \text{ mol L}^{-1}$  ethanol,  $T = 25^\circ\text{C}$  and for (a) Ni/aHC sample and (c) NiO/HC sample. Backgrounds were collected at  $0.0 \text{ V}$  (Hg/HgO). (b) Acetaldehyde and acetate band intensities as a function of the potential for the Ni/aHC sample.

increase from *ca.*  $0.5$ – $0.6 \text{ V}$  vs. Hg/HgO. This is consistent with the rapidly increasing of the net current density associated with the EOR observed in Fig. 7c and the cathodic peak observed in Fig. 7a. Regarding the band intensity at  $931 \text{ cm}^{-1}$  associated with acetaldehyde, it can be seen a small increase from  $0.3 \text{ V}$  vs. Hg/HgO reaching a maximum at  $0.5 \text{ V}$  and then decreased to minimum values from  $0.6 \text{ V}$ . However, the acetaldehyde band intensity is much smaller than observed for the acetate ion from  $0.6 \text{ V}$ . Therefore, if acetaldehyde is formed as reaction product of EOR, it does not occur in large extension, and if it was an intermediary reaction it should happen rapidly.

In summary, based on the spectroelectrochemical and electrochemical analyses, and in the literature information [2,6,70], a reaction pathway of the EOR on Ni/aHC electrocatalyst can be proposed as follow:



The FTIR spectra obtained for the NiO/HC sample at different potentials are shown in Fig. 9c. Significant peaks, associated with the EOR products or ethanol consumption are not detected at any potential. This is consistent with the electrochemical analysis results where the lower catalytic activity of the NiO/HC sample was confirmed (Fig. 8c). Therefore, the possible EOR products cannot be detected (at least under the *in-situ* ATR-FTIR experimental analysis conditions) that maybe due to the lower concentration of the possibly generated EOR products.

#### 4. Conclusions

A simple, low cost, and environmental friendly method for metallic nickel based electrocatalyst preparation was investigated. In the first stage of the proposed method, NiO nanoparticles supported on hydrothermal carbon (NiO/HC) were obtained. In the next step, due to the occurrence of a NiO carbothermal reduction and the hydrothermal carbon activation, an activated hydrothermal carbon supported nickel catalyst (Ni/aHC) was obtained. The electrochemical characterization of the Ni/aHC sample showed that this sample is suitable for its use as electrocatalyst for ethanol electro-oxidation in alkaline medium. The maximum developed oxidation current densities are comparable to those reported for other types

of catalysts for the EOR in the same medium. Cyclic voltammetry in NaOH solution, in the presence and in the absence of ethanol, infers the participation of the (NiO)OH species in the EOR. This species was formed at 0.47 V vs Hg/HgO electrode. The *in-situ* ATR-FTIRS analysis demonstrate that acetate ion is the most important product of the EOR on Ni/aHC in alkaline medium. This product begins to form appreciably from 0.5–0.6 V vs. Hg/HgO which is consistent with the results of cyclic voltammetry performed in the presence of ethanol.

## Acknowledgements

The present work was carried out with support of CAPES (project CAPES/UdelaR N° 044/2011), Brazilian Government entity focused in human resources formation. The authors would also like to thank the CNPq. A. Cuña thanks the Brazilian CAPES for the grant received (Bolsista CAPES/Brasil). C. Reyes Plascencia gratefully acknowledged at National Council of Science and Technology in Mexico (CONACYT) her PhD scholarship.

## References

- [1] D.R.M. Godoi, H.M. Villullas, F.-C. Zhu, Y.-X. Jiang, S.-G. Sun, J. Guo, L. Sun, R. Chen, *J. Power Sources* 311 (2016) 81–90.
- [2] F. Muench, M. Oezaslan, M. Rauber, S. Kaserer, A. Fuchs, E. Mankel, J. Brötz, P. Strasser, C. Roth, W. Ensinger, *J. Power Sources* 222 (2013) 243–252.
- [3] S. Sun, Z. Jusys, R.J. Behm, *J. Power Sources* 231 (2013) 122–133.
- [4] A.N. Geraldes, D.F. da Silva, E. Segura Pino, J.C. Martins da Silva, R.F. Brambilla de Souza, P. Hammer, E.V. Spinacé, A. Oliveira Neto, M. Linardib, M. Coelho dos Santos, *Electrochim. Acta* 111 (2013) 455–465.
- [5] R.M. Modibedi, T. Masombuka, M.K. Mathe, *Int. J. Hydrogen Energy* 36 (2011) 4664–4672.
- [6] E. Antolini, E.R. Gonzalez, *J. Power Sources* 195 (2010) 3431–3450.
- [7] Y.S. Li, T.S. Zhao, Z.X. Liang, *J. Power Sources* 187 (2009) 387–392.
- [8] E. Antolini, *J. Power Sources* 170 (2007) 1–12.
- [9] E. Peled, V. Livshits, T. Duvdevani, *J. Power Sources* 106 (2002) 245–248.
- [10] R. Dillon, S. Srinivasan, A.S. Aricò, V. Antonucci, *J. Power Sources* 127 (2004) 112–126.
- [11] Y. Li, Y. He, *RSC Adv.* 4 (2014) 16879–16884.
- [12] Y.S. Li, Y.L. He, W.W. Yang, *Int. J. Hydrogen Energy* 38 (2013) 13427–13433.
- [13] Y.S. Li, T.S. Zhao, *Int. J. Hydrogen Energy* 37 (2012) 15334–15338.
- [14] Y.S. Li, T.S. Zhao, *Int. J. Hydrogen Energy* 37 (2012) 4413–4421.
- [15] Y. Li, Y. He, *Electrochim. Soc* 163 (2016) F663–F667.
- [16] A. Zalineva, A. Serov, M. Padilla, U. Martinez, K. Artyushkova, S. Baranton, C. Coutanceau, P. Atanassov, *Electrochim. Commun.* 57 (2015) 48–51.
- [17] Q. He, W. Chen, S. Mukerjee, S. Chen, F. Laufek, *J. Power Sources* 187 (2009) 298–304.
- [18] L.-S. Jou, J.-K. Chang, T.-J. Twhang, I.-W. Sun, *J. Electrochim. Soc.* 156 (2009) D193–D197.
- [19] C. Xu, P.K. Shen, Y. Liu, *J. Power Sources* 164 (2007) 527–531.
- [20] C. Xu, Z. Tian, P.K. Shen, S.P. Jiang, *Electrochim. Acta* 53 (2008) 2610–2618.
- [21] D. Chu, J. Wang, S. Wang, L. Zha, J. He, Y. Hou, Y. Yan, H. Lin, Z. Tian, *Catal. Commun.* 10 (2009) 955–958.
- [22] J.-W. Kim, S.-M. Park, *J. Electrochim. Soc.* 146 (1999) 1075–1080.
- [23] J.-W. Kim, S.-M. Park, *J. Electrochim. Soc.* 150 (2003) E560–E566.
- [24] D.T. Shieh, B.J. Hwang, *J. Electrochim. Soc.* 142 (1995) 816–823.
- [25] S. Jongsomjit, P. Prapainainar, K. Sombatmankhong, *Solid State Ionics* 288 (2016) 147–153.
- [26] L. Silveira Parreira, J.C. Martins da Silva, M. D'Villa-Silva, F. Carmona Simões, S. Garcia, I. Gaubeur, M.A. Liutheviene Cordeiro, E.R. Leite, M. Coelho dos Santos, *Electrochim. Acta* 96 (2013) 243–252.
- [27] P. Serp, B. Machado, *Nanostructured Carbon Materials for Catalysis*, Royal Social of Chemistry, Londres, 2015.
- [28] E. Antolini, *Appl. Catal. B* 88 (2009) 1–24.
- [29] J. Asgardi, J.C. Calderón, F. Alcaide, A. Querejeta, L. Calvillo, M.J. Lázaro, G. García, E. Pastor, *Appl. Catal. B* 168 (2015) 33–41.
- [30] L. Yuan, L. Jiang, J. Liu, Z. Xia, S. Wang, G. Sun, *Electrochim. Acta* 135 (2014) 168–174.
- [31] E.L. Silva, M.R. Ortega Vega, P.S. Correa, A. Cuña, N. Tancredi, C.F. Malfatti, *Int. J. Hydrogen Energy* 39 (2014) 14760–14767.
- [32] L. Calvillo, V. Celorio, R. Moliner, A.B. Garcia, I. Camean, M.J. Lazaro, *Electrochim. Acta* 102 (2013) 19–27.
- [33] N. Nakagawa, Y. Ito, T. Tsujiguchi, H. Ishitobi, *J. Power Sources* 248 (2014) 330–336.
- [34] L.M. Ombaka, P. Ndungu, V.O. Nyamori, *Catal. Today* 217 (2013) 65–75.
- [35] Y. Li, J. Lv, Y. He, *J. Electrochim. Soc.* 163 (2016) F424–F427.
- [36] A. Cuña, N. Tancredi, J. Bussi, V. Barranco, T.A. Centeno, A. Quevedo, J.M. Rojo, *J. Electrochim. Soc.* 161 (2014) A1806–1811.
- [37] A. Cuña, N. Tancredi, J. Bussi, C. Deiana, M.F. Sardella, V. Barranco, J.M. Rojo, *Waste Biomass Valorization* 5 (2014) 305–313.
- [38] M. Sevilla, W. Gu, C. Falco, M.M. Titirici, A.B. Fuertes, G. Yushin, *J. Power Sources* 267 (2014) 26–32.
- [39] M. Sevilla, J.A. Macia-Agullo, A.B. Fuertes, *Biomass Bioenergy* 35 (2011) 3152–3159.
- [40] A. Funke, F. Ziegler, *Biofuels Bioprod. Biorefin.* 4 (2010) 160–177.
- [41] D. Knezevic, W. van Swaaij, S. Kersten, *Hydrothermal conversion of biomass: I. glucose conversion in hot compressed water*, *Ind. Eng. Chem. Res.* 49 (2010) 104–112.
- [42] H. Xiong, M. Moyo, M.A. Motchelaho, Z.N. Tetana, S.M.A. Dube, L.L. Jewell, N.J. Coville, *J. Catal.* 311 (2014) 80–87.
- [43] J. Matos, M. Rosales, R. Demir-Cakanb, M.M. Titirici, *Appl. Catal. A* 386 (2010) 140–146.
- [44] T. Iwasita, F.C. Nart, *Prog. Surf. Sci.* 55 (1997) 271–340.
- [45] T. Iwasita, G.A. Camara, in: S.-G. Sun, P.A. Christensen, A. Wieckowski (Eds.), *In-situ Spectroscopic Studies of Adsorption at the Electrode and Electrocatalysis*, Elsevier B.V, Amsterdam, 2007, pp. 33–61.
- [46] R.F.B. De Souza, J.C.M. Silva, F.C. Simoes, M.L. Calegaro, A.O. Neto, M.C. Santos, *Int. J. Electrochim. Sci.* 7 (2012) 5356–5366.
- [47] M.E. Paulino, L.M.S. Nunes, E.R. Gonzalez, G. Tremiliosi-Filho, *Electrochim. Commun.* 52 (2015) 85–88.
- [48] M.H.M.T. Assumpção, J. Nandinha, G.S. Buzzo, J.C.M. Silva, E.V. Spinacé, A.O. Neto, R.F.B. De Souza, *J. Power Sources* 253 (2014) 392–396.
- [49] J.C.M. Silva, L.S. Parreira, R.F.B. De Souza, M.L. Calegaro, E.V. Spinacé, A. Oliveira Neto, M.C. Santos, *Appl. Catal. B* 110 (2011) 141–147.
- [50] R.F.B. De Souza, L.S. Parreira, J.C.M. Silva, F.C. Simoes, M.L. Calegaro, M.J. Giz, A.O. Neto, M.C. Santos, *Int. J. Hydrogen Energy* 36 (2011) 11519–11527.
- [51] M. Heinen, Z. Jusys, R.J. Behm, *J. Phys. Chem.* 114 (2010) 9850–9864.
- [52] L. Zhang, J. Mu, Z. Wang, G. Li, Y. Zhang, Y. He, *J. Alloys Compd.* 671 (2016) 60–65.
- [53] M. Salavati-Niasari, F. Mohandes, F. Davar, M. Mazaheri, M. Monemzadeh, N. Yavarinia, *Inorg. Chim. Acta* 362 (2009) 3691–3697.
- [54] C. Li, Y.-W. Chen, *Thermochim. Acta* 256 (1995) 457–465.
- [55] L. Wang, H. Tian, D. Wang, X. Qin, G. Shao, *Electrochim. Acta* 151 (2015) 407–414.
- [56] E. Arico, F. Tabuti, F.C. Fonseca, D.Z. de Florio, A.S. Ferlauto, *J. Therm. Anal. Calorim.* 97 (2009) 157–161.
- [57] A. Paravanoor, R. Ranjusha, A.M. Asha, R. Vani, S. Kalluri, K.R.V. Subramanian, *Chem. Eng. J.* 220 (2013) 360–366.
- [58] W. Xing, S. Qiao, X. Wu, X. Gao, J. Zhou, S. Zhuo, S.B. Hartono, D. Hulicova-Jurcakova, *J. Power Sources* 196 (2011) 4123–4127.
- [59] M.A. Goula, N.D. Charisiou, K.N. Papageridis, A. Delimitis, E. Pachatouridou, E.F. Iliopoulos, *Int. J. Hydrogen Energy* 40 (2015) 9183–9200.
- [60] W. Chu, M. Ran, X. Zhang, N. Wang, Y. Wang, H. Xie, X. Zhaod, *J. Energy Chem.* 22 (2013) 136–144.
- [61] C. Xu, Y. Hu, J. Rong, S. Ping Jiang, Y. Liu, *Electrochim. Commun.* 9 (2007) 2009–2012.
- [62] B.V. L'vov, *Thermochim. Acta* 360 (2000) 109–120.
- [63] H. Marsh, R.F. Rodríguez-Reinoso, *Activated Carbons*, Elsevier Oxford, UK, 2006.
- [64] P. Moravec, J. Smolík, H. Keskinen, J.M. Mäkelä, S. Bakardjieva, V.V. Levanský, *Mater. Sci. Appl.* 2 (2011) 258–264.
- [65] C. Wang, P. Zhai, Z. Zhang, Y. Zhou, J. Zhang, H. Zhang, Z. Shi, R.P.S. Han, F. Huang, Ding Ma, *J. Catal.* 334 (2016) 42–51.
- [66] F. Davar, Z. Fereshteh, M. Salavati-Niasari, *J. Alloys Compd.* 476 (2009) 797–801.
- [67] I. Czekaj, F. Loviat, Fabio Raimondi, J. Wambach, S. Biollaz, A. Wokaun, *Appl. Catal. A* 329 (2007) 68–78.
- [68] R. Fernández, J. Estelle, Y. Cesteros, P. Salagre, F. Medina, J.E. Sueiras, J.L. Garcia Fierro, *J. Mol. Catal. A: Chem.* 119 (1997) 77–85.
- [69] M.A. Sattar, B.E. Conway, *Electrochim. Acta* 14 (1969) 695–710.
- [70] M. Fleischmann, K. Korinek, D. Pletcher, *J. Electroanal. Chem. Interfacial Electrochem.* (1971) 39–49.
- [71] Z. Liu, Z. Li, F. Wang, J. Liu, J. Ji, J. Wang, W. Wang, S. Qin, L. Zhang, *Mater. Lett.* 65 (2011) 3396–3398.
- [72] M.D. Obradovic, Z.M. Stancic, U.C. Lacnjevac, V.V. Radmilovic, A. Gavrilovic-Wohlmuthere, V.R. Radmilovic, S. Lj Gojkovic, *Appl. Catal. B* 189 (2016) 110–118.
- [73] S.Y. Shen, T.S. Zhao, J.B. Xu, Y.S. Li, *J. Power Sources* 195 (2010) 1001–1006.
- [74] T. Maiyalagan, K. Scott, *J. Power Sources* 195 (2010) 5246–5251.
- [75] Z. Zhang, L. Xin, K. Sun, W. Li, *Int. J. Hydrogen Energy* 36 (2011) 12686–12697.
- [76] M.A. Sattar, B.E. Conway, *Electrochim. Acta* 14 (1969) 695–710.
- [77] X. Fang, L. Wang, P.K. Shen, G. Cui, C. Bianchini, *J. Power Sources* 195 (2010) 1375–1378.
- [78] S.C. Chang, L.-M. Leung, M.J. Weaver, *J. Phys. Chem.* 94 (1990) 6013–6021.
- [79] L.-W. Leung, S.C. Chang, M.J. Weaver, *J. Electroanal. Chem.* 266 (1989) 317–336.
- [80] E.K. Plyler, *J. Res. Natl. Bur. Stand.* 48 (1952) 281–286.
- [81] J.C. Morris, *J. Chem. Phys.* 11 (1943) 230–235.